Wear and Corrosion Behaviors of Inconel 625-Cladded Layer on P460N Steel in Different Environments

MASOUD ZAFARI, MOJTABA ESMAILZADEH, SEYEDEH NARJES HOSSEINI, and E. SHAFIEI

In this research, an investigation of the microstructure, hardness, corrosion, and wear behavior of Inconel 625-cladded layer on P460N Steel fabricated by Gas Tungsten Arc Welding has been done. Microstructural examinations using optical microscopy, scanning electron microscopy (with energy dispersive X-ray spectroscopy), and X-ray diffraction revealed the epitaxially grown dendrites with the average primary and secondary dendrite spacing of 17 and 9 μm in the cladded layer, and the Widmanstatten ferrites in the interface zone between the heat-affected zone and cladded layer. The hardness showed its maximum value of 230 HV at a depth of about 500 μm from the cladded layer's surface, due to the more uniform distribution of precipitate particles and elements in this region. The Tafel and Cyclic polarization tests in the saline solution indicated that cladding of P460N Steel with Inconel 625 resulted in reducing the corrosion rate by about three times. The comparative pin-on-disk wear test demonstrated a decreasing wear coefficient and wear rates in cladded samples at low wear forces of 22.5 N. In contrast, the wear was intensified with increasing loading force to 45 N due to severe three-body abrasion. Although the wear coefficients were reduced in the water environment, it led to further destruction of the samples as a result of cavitation.

I. INTRODUCTION

DUE to the unique physical and mechanical properties such as strength, abrasion resistance, and high corrosion, Inconel 625 alloy has found wide applications.[1] The existence of austenitic matrix (Υ) along with FCC carbides (MC, $M_{23}C_6$) precipitations and reinforcing phases such as Υ'' phase (Ni_3Nb_x) and Laves phase are the main reasons for these excellent properties.[2] On the other hand, given the high cost of bulk production and its relatively good weldability, cladding techniques of Inconel 625 alloy have been extensively developed. Among different methods, some techniques such as explosive welding,[3] thermal spray,[4] laser cladding,[5] and Gas Tungsten Arc Welding (GTAW) cladding[6,7] have been more attractive to industries and scientists. The GTAW technique is more common than other methods, because it has lower equipment costs and better accessibility and compatibility with a wide range of materials.

Longlong *et al.*[8] have evaluated the microstructure and corrosion resistance of Inconel 625 cladded on AISI 4130 by GTAW. They claimed that a cladded layer of the second pass leads to better corrosion resistance. Also, dilution of elements happens in high heat input parameters. Fesharaki *et al.*[2,9] have compared the Inconel 625-cladded layers obtained from laser and GTAW techniques. The results showed GTAW cladding technique could produce a flawless layer with higher hot corrosion resistance than the base metal. The formation of the $NiCr_2O_4$ phase has led to improving corrosion properties. Silwal *et al.*[6] have characterized the Inconel 625-cladded layer on 347 stainless steel by GTAW. They further evaluated the concentration and dilution changing of elements. Wang *et al.*[10] also utilized the GTAW method to fabricate the Inconel 625 deposited layer. Due to the inhomogeneity of microstructure, hardness and strength of the last layers were increased. Literature studies indicate that much attention has been focused on the microstructure, chemical composition, and corrosion behavior of Inconel 625 cladded.

MASOUD ZAFARI is with the Iranian Marine Industries, Bandar-Abbas, Iran and with the Department of Materials Science and Engineering, Islamic Azad University, Bandar Abbas Branch, Bandar Abbas, Iran. MOJTABA ESMAILZADEH and SEYEDEH NARJES HOSSEINI are with the Department of Mechanical Engineering, Persian Gulf University, Bushehr, 75169, Iran. Contact e-mail: m.esmaeilzade@pgu.ac.ir E. SHAFIEI is with the Department of Materials Science and Engineering, Islamic Azad University. Contact e-mail: shafiei.ehsan.mse@gmail.com

Iwabuchi[11] has investigated the wear behavior of Inconel 625 at different pressures and temperatures. It is reported that the wear resistance was increased at high temperature and low pressure. In other words, forming a glaze oxide at high temperatures has resulted in reducing the wear volume and coefficient of friction. Also, Kashani *et al.*[12] have cladded AISI H11 tool steel with different electrodes such as Inconel 625 by GTAW. They have claimed that the bearing oxide layer has formed at high temperatures, and so the wear resistance has increased. Desale *et al.*[13] have evaluated erosion wear behavior of Inconel 625 laser cladded on 316L stainless steel. Inconel 625 clad surface showed little improvement in erosion wear resistance. Chakraborty *et al.*[14] have studied the wear behavior of three Ni hard-facing alloys. It is been claimed that chemical composition changes due to dilution, effect volume fraction, and morphology, thereby controls the hardness and abrasion resistance. Verdi *et al.*[15] have studied local wear behavior of Cr_3C_2/Inconel 625 composite layer. They have reported that reinforcing particles in the cladding layer prevent severe local plastic deformation during wear.

Most of the literature works have focused on the wear behavior of Inconel alloys in air environment, and fewer studies have been done concerning the tribological properties of these alloys in other environments. Wang and co-workers reported that increasing the seawater pressure increases the wear rate of Inconel 625 in terms of a first-order exponential function, and the dominant wear mechanism is delamination.[16]

Chen *et al.* have showed that although the corrosion of seawater accelerates the wear loss of Inconel 625, the friction coefficients were smaller compared to sliding in distilled water. Increasing the loading also decreased the wear coefficients.[17] The influence of environment on wear rate and mechanism depends on how far it affects the metal-to-metal contact due to the formation of different metallic components such as oxides, nitrides, *etc.*, at the sliding interface.

However, there are limited results available for the wear behavior of Inconel 625 cladded at different environments. Based on this fact, in the present research, the wear behaviors and wear mechanisms of cladded Inconel 625 alloy under different environments are investigated. And the correlation between the wear behaviors of tested materials and the environmental conditions are evaluated. Besides, the corrosion behavior of the base metal and cladded layer has been studied in simulated seawater.

II. MATERIALS AND METHODS

A. *Materials*

The chemical composition of the substrate material used, P460N steel, measured by a PMI MASTER SMART spectrometer is listed in Table I. The nominal chemical composition of filler wire (diameter 2.4 mm) of Inconel 625 (ERNiCrMo3) used for cladding is also mentioned in Table I.

B. *Cladding*

For the cladding of P460N steel with Inconel 625, GTAW process has been used. Before welding, the surface of the substrate material was sanded and cleaned, and then it was preheated up to 150 °C. Table II shows the welding parameters employed in the present study. The mean welding heat input according to the equation: HI = 0.48 (V.I/S) was calculated to be 680 J/mm.

C. *Microstructural and Phase Analysis*

The sample preparation for microstructural analysis of the base metal, weld metal, and heat-affected zone regions was done according to ASTM E3:11 standards. The samples were ground with 80 to 2000 grit size SiC sandpapers, polished with Al_2O_3 powder in an aqueous suspension, and finally etched in 2 pct Nital and Glyceregia. Microstructural observations were carried out using RMM-2 Radical Metallurgical Microscope and MIRA-3 VEGA\\TESCAN SEM Microscope (at 15 kV). FESEM, EDS, and XRD analysis (include Cu $K_\alpha \lambda = 1.54$ Å) was also employed to characterize the samples.

D. *Hardness*

The hardness values in the cladded surface, interface region, and substrate were evaluated by the Vickers microhardness test method based on ISO 6507-1 standard. The hardness profile across the interface was plotted using a diamond pyramid indenter with a load of 300 gf and a dwell time of 10 to 15 seconds.

E. *Corrosion Behavior*

Electrochemical corrosion resistant properties of the P460N steel and Inconel 625 surfaces were evaluated by Tafel and Cyclic polarization tests in 3.5 wt pct NaCl water solutions at room temperature (25 °C) using an Auto-Lab potentiometer controlled by Nova software. The tests were carried out according to ASTM G-102-89 and ASTM G-61-86 Standards. The samples were mounted in epoxy resin, and before the corrosion test, the surfaces were sanded (100 to 1500 grit) and cleaned with distilled water and acetone. Before the potentiodynamic polarization test, the samples were immersed in the NaCl solution to obtain open circuit potential (OCP) for 60 minutes. Then, the corrosion measurements were carried out (regarding the saturated calomel electrode, SCE) by scanning from 250 mV more negative than the OCP at a scan rate of 0.5 mV/s.

Besides, an immersion test has been performed to evaluate the corrosion behavior of samples accurately. Different specimens were immersed in 1 molar hydrochloric acid solution for 1000 hours. The corroded samples were removed from the solution at different times to record weight changes and study the corroded surfaces. Before weight measurements, the corrosion

Table I. Chemical Composition (Wt Pct) of the Base and Filler Material

Material	Fe	Ni	C	Mn	Si	Cr	Nb	V	P	S	Mo	Al
P460N	97.09	0.19	0.17	1.49	0.41	0.08	0.004	0.077	0.011	0.005	—	—
Inconel 625	0.25	64.75	0.02	0.035	0.055	22.65	3.5	—	0.001	—	8.6	0.2

Table II. Process Parameters for GTAW Cladding

DCEN Current (A)	Voltage (V)	Welding Speed (mm/s)	Electrode Diameter (mm)	Shielding Gas (flow rate)	Minimum Arc Length (mm)
90 to 110	12 to 14	1	2.4	Ar (20 L/min)	2

Table III. The Process Parameters and Names of Samples Used in the Wear Tests

Sample	F (N)	V (m/s)	V (rpm)	Sliding (m)	Wear Environment
BM45-2	45	0.5	954.9	200	air
BM45-4	45	0.5	367.3	400	air
BM45-8	45	0.5	154	800	air
BM22.5-2	22.5	0.5	238.7	200	air
BM22.5-4	22.5	0.5	367.3	400	air
BM22.5-8	22.5	0.5	144.7	800	air
C45-2	45	0.5	198.9	200	air
C45-4	45	0.5	280.9	400	air
C45-8	45	0.5	238.7	800	air
C22.5-2	22.5	0.5	954.9	200	air
C22.5-4	22.5	0.5	176.8	400	air
C22.5-8	22.5	0.5	298.4	800	air
W-BM45-4	45	0.5	159.1	400	distilled water
W-BM45-8	45	0.5	265.2	800	distilled water
W-C45-4	45	0.5	191	400	distilled water
W-C45-8	45	0.5	682.1	800	distilled water

BM: Base Metal, C: Cladded, W: Water.

products were cleaned from the samples surfaces by soft sanding and floating in an ultrasonic bath. Finally, each sample was weighed at least three times.

F. Wear Behavior

The wear behavior of the Inconel 625-cladded surface was compared to P460N steel using a conventional pin-on-disk wear testing machine (TRM 500 Tribometer machine—WAZAU, Germany). The reciprocal sliding was fixed by rubbing a standard EN31 hard steel disk with a diameter of 80 mm against the cylindrical pin samples with a diameter of 12 mm. The applied test parameters and names of samples used in the wear tests are summarized in Table III.

The coefficients of friction were recorded continuously during the experiments. The initial and final weights of the samples were measured using a digital-weighing balance. Each experiment was repeated at least two times with a new steel disk and polished samples for checking the repeatability of single

measurements, and average results were reported. The wear surface morphology of the samples was examined under a Philips XL-30 SEM Microscope at 25 kV.

III. RESULTS AND DISCUSSION

A. Microstructure Analysis

Figure 1 shows optical and scanning electron microscopy images of P460N ferrite-pearlite steel. The perlite phase is distributed as relatively continuous islands in the ferrite matrix. The effects of deformation are still visible caused by pre-rolled annealing. The SEM image illustrates the annealed hypoeutectoid microstructure of the P460N steel alloy clearly. Further observations indicated defects such as precipitations, porosities, etc.

Figure 2(a) represents a sharp interface between the cladded layer/base metal. Different regions can be seen such as the cladded layer, interface, heat-affected zone, and base metal. The microstructure of base metal has been described previously.
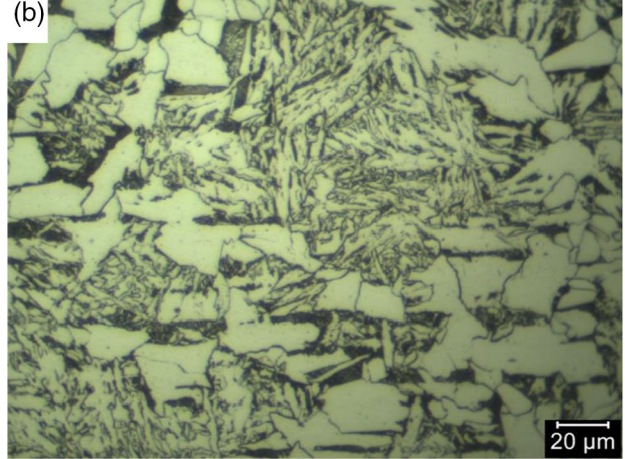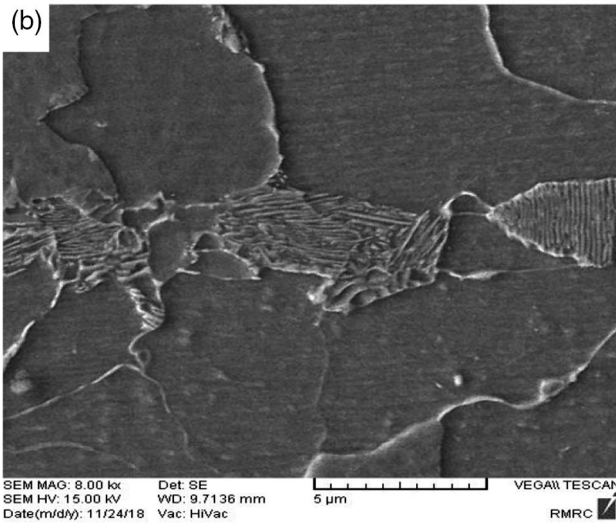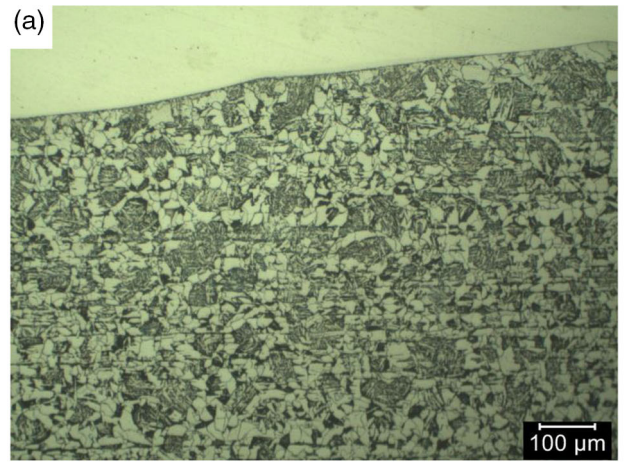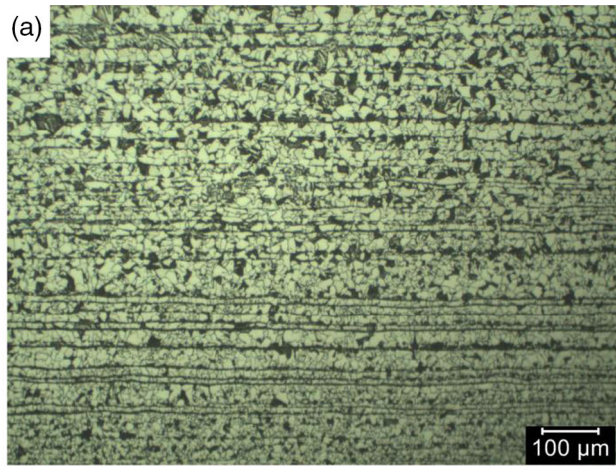
Fig. 1—Microstructure of P460N base metal steel (*a*) OM image, (*b*) SEM image.

Figure 2(b) shows that the average grain size of HAZ microstructures has increased due to incurring high heat energy. But the microstructural form of the interface has been changed significantly compared to the base metal and HAZ. This region has been formed between HAZ/cladded layer areas. The Widmanstatten ferrites were found due to partial melting and rapid solidification of the microstructure in this zone.

In all specimens, the cladded layer has a mostly dendritic structure, which is epitaxially grown from the substrate to the welding center (Figure 2(c)). Due to changes in the temperature gradient in the welding pool during the cladding process, local solidification has occurred in some areas, and fine dendrites were also visible. The same results were reported for the Inconel 625-cladded layer by.[6,18] The results of image processing showed that the average primary and secondary dendrite spacing was 17 and 9 μm, respectively.
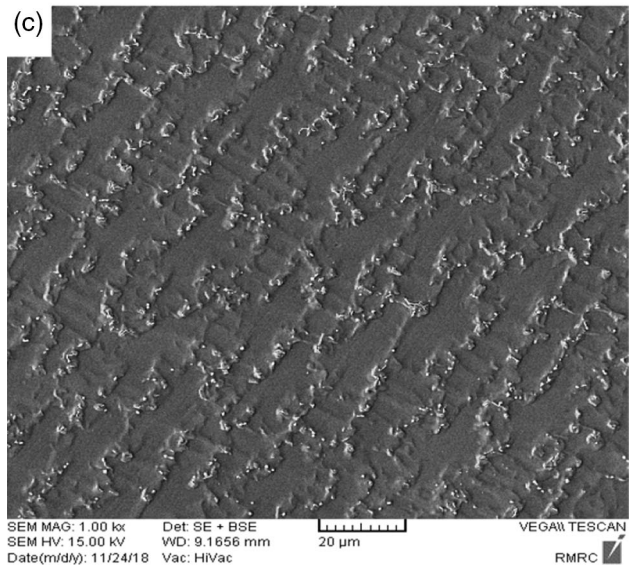
Fig. 2—The microstructure of (*a*) cladded layer and base metal interface, (*b*) HAZ, (*c*) Inconel 625-cladded layer.
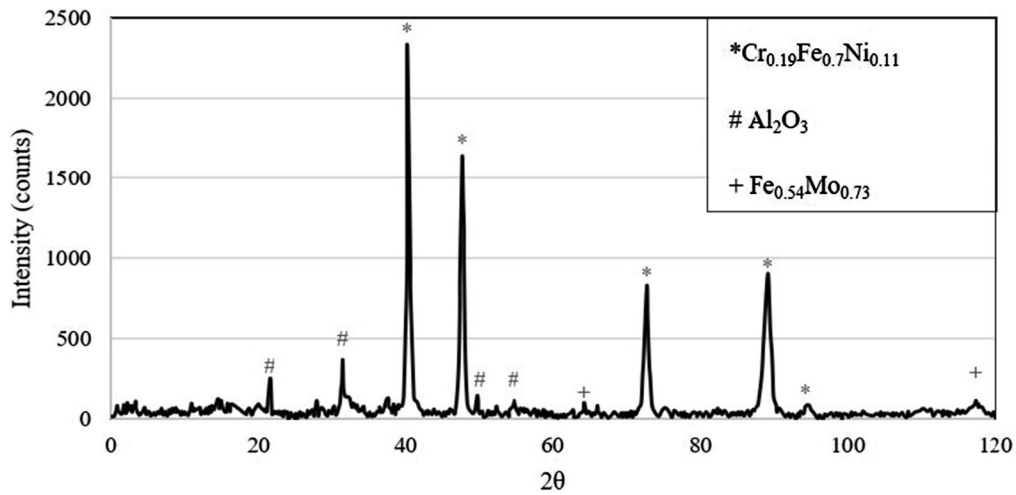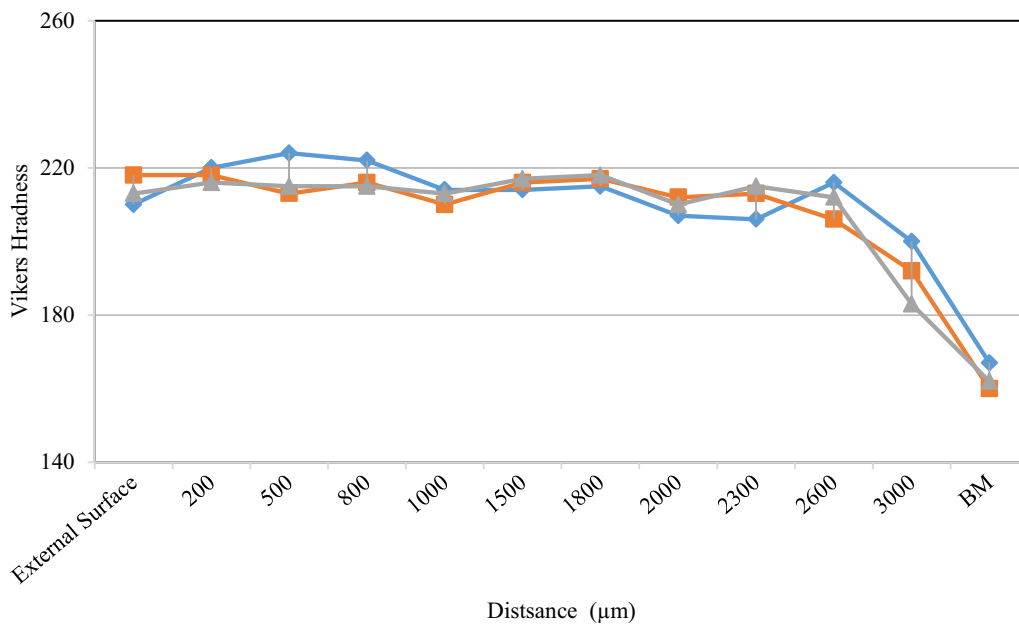
Fig. 3—XRD pattern of Inconel 625-cladded layer.

Fig. 4—Hardness number changing from external surface to base metal.

On the other side, XRD results show the presence of precipitations with $Fe_{0.54}Mo_{0.73}$ and $Cr_{0.19}Fe_{0.7}Ni_{0.11}$ compound in Figure 3. However, weak peaks of Al_2O_3 have also been observed. It seems that aluminum oxide formation and confinement will be inevitable even with the welding zone's slightest control.

B. Hardness Test

Due to the importance of surface hardness in the wear behavior of materials, this property has been investigated with accuracy. The results of the Vickers hardness are presented in Figure 4. It can be seen that the average hardness of the cladded layer and the base metal were 215 and 160 HV, respectively. Therefore, the hardness of the Inconel 625-cladded layer is about 2.5 times the base metal. A closer examination of the hardness results illustrates that the hardness number has a uniform distribution from the outer surface to near the base metal interface. These results predict the uniform distribution of elements across the cladded layer. Figure 5(a) illustrates the EDS map scan of Figure 2(c). It can be concluded that the main elements (Ni, Cr, and Mo) of the cladded layer have a uniform distribution.

Figure 5 shows the distribution of elements such as Ni, Cr, Fe, Mn, and Mo in the interface of the cladded layer and steel base metal. In this area, the concentration of elements such as Ni, Cr, Mn, and Mo gradually decreased, and the Fe concentration increased dramatically.
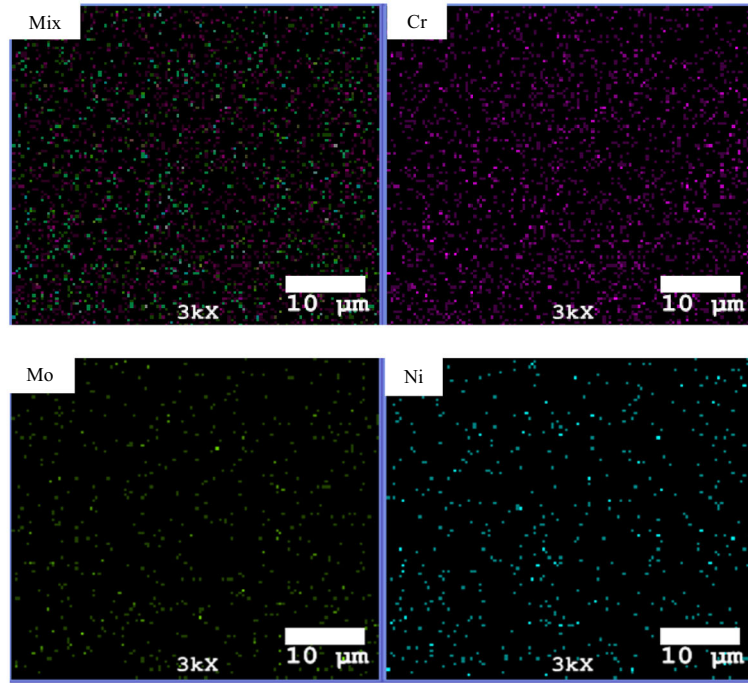
(a)
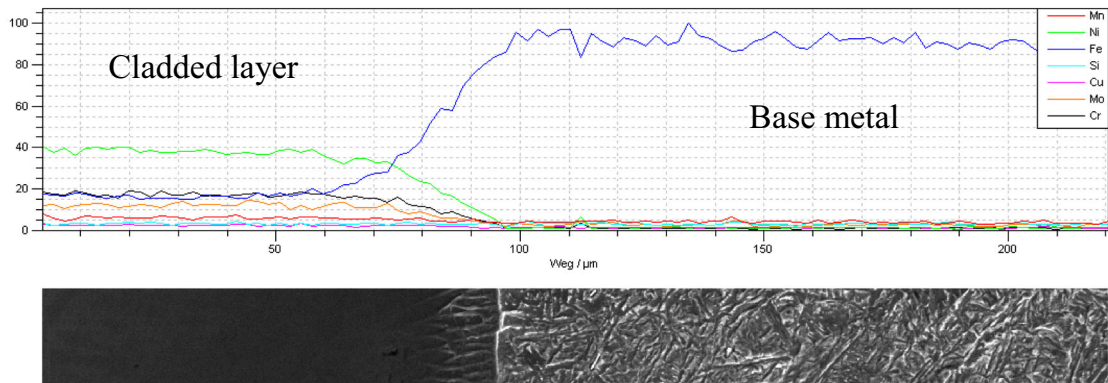
(b)

Fig. 5—Result of (*a*) EDS map scan of cladded layer, (*b*) EDS line scan from cladded layer to base metal.

C. *Corrosion Test*

Figure 6 shows the polarization curve of P460N steel and Inconel 625 as the base metal and cladded layer in 3.5 pct NaCl solution, respectively. The quantitative results of these curves have been extracted by NOVA software and are listed in Table IV.

The comparison of E_{corr} values indicates that the Inconel 625-cladded layer has a lower tendency to corrosion than P460N steel as the base metal. Also, the i_{corr} values show that the corrosion rate of the base metal is about 2.7 times greater than the cladded layer. The corrosion rate (CR) was measured by Eq. [1]:

$$CR = \frac{i_{corr} \cdot K \cdot E_w}{\sigma \cdot A},$$ [1]

where i_{corr} is the corrosion current in amperes, K is a constant that defines the units for the corrosion rate, E_w is the equivalent weight in g/equivalent, σ is the density in g/cm^3, A is the sample area in cm^2.

To ensure the results, the cyclic polarization test was done for the cladded layer and, the final results are listed in Table V. There is a fairly good agreement between the corrosion rates of linear and cyclic polarization.

Excessive amount of molybdenum element contributes to the inactivation of the surface, which increases the corrosion resistance of the substrate, thus preventing the deterioration of chlorine ions in the environment. Various reports have been published on the effect of Mo on the corrosion behavior of alloys. Wang *et al.*[19] have concluded that the corrosion resistance of the coating containing Mo is better than
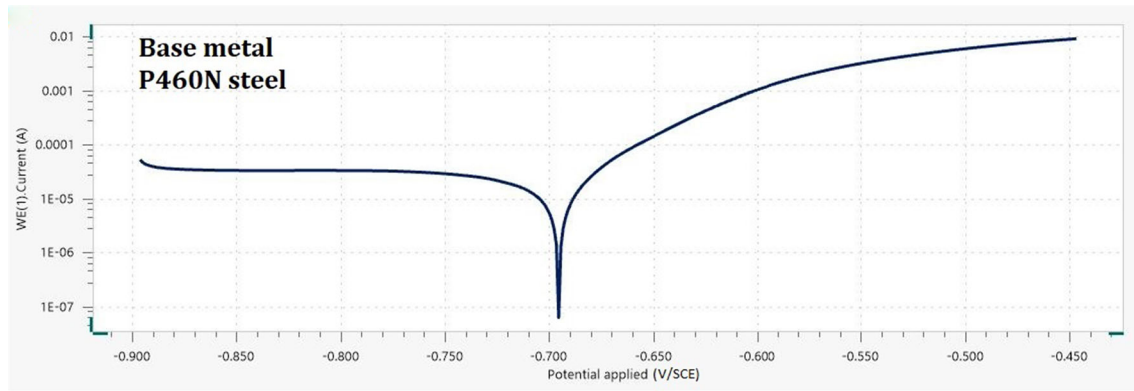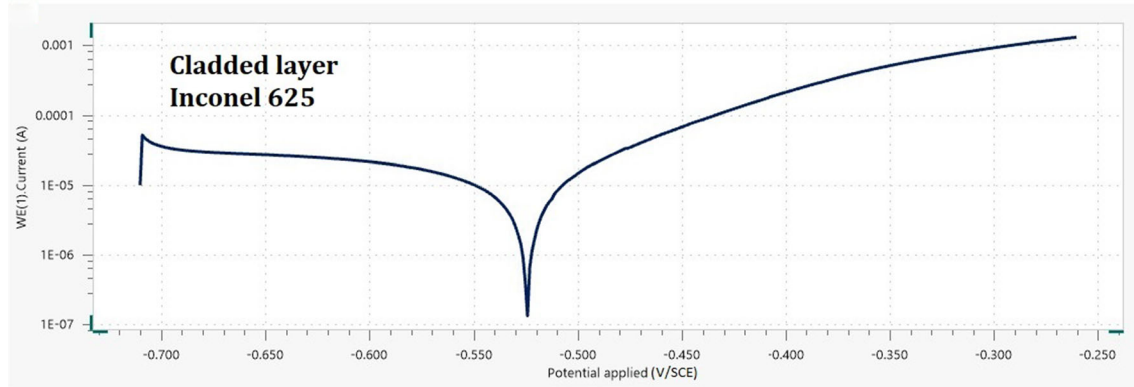
Fig. 6—Polarization test of (*a*) base metal P460N steel, (*b*) cladded layer of Inconel 625.

Table IV. Corrosion Test Results of Polarization Test

Sample	E_{corr} (v)	b_a (V/dec)	b_c (V/dec)	i_{corr} (A/cm^2)	CR (mpy)
P 460N	−0.6956	0.12	0.12	3.5599×10^{-5}	16.29
Cladded Inconel 625	−0.52471	0.12	0.12	1.3154×10^{-5}	6.02

Table V. Corrosion Parameters of Inconel 625-Cladded Layer From Cyclic Polarization

i_{corr} (μA/cm^2)	b_c (mV/dec)	b_a (mV/dec)	E_{corr} (mV)	E_p (mV)	E_b (mV)	C.R (mpy)
3.689	243.008	60.714	−616.775	290.2	1210	5.78

that of the Mo-free coating. Ramkumar *et al.*[20] have reported about the positive effect of Mo-reach fillers on improving hot corrosion resistance of welded Inconel 718. Also, the lower dilution of Fe in the Inconel cladded layer leads to increasing its corrosion resistance. In other words, the corrosion resistance of the outer surface of the cladded layer is much higher than its inner layers. It should be noted that in addition to element distribution, morphological changes are also very effective in the improvement of materials' corrosion behavior.

The weight changes resulting from the immersion test are shown in Figure 7. Results show that the base metal corrosion rate is higher than the cladded specimens during 1000 hours of immersion. Figure 8 illustrates the optical images of the corroded surfaces after 1000 hours of immersion test. Fewer corrosion cavities are observed at the surface of the cladded samples. The same results have been reported by Kim,[21] Ramkumar,[22] and Xu *et al.*[23] for the corrosion behavior of the welded layer of Inconel 625.
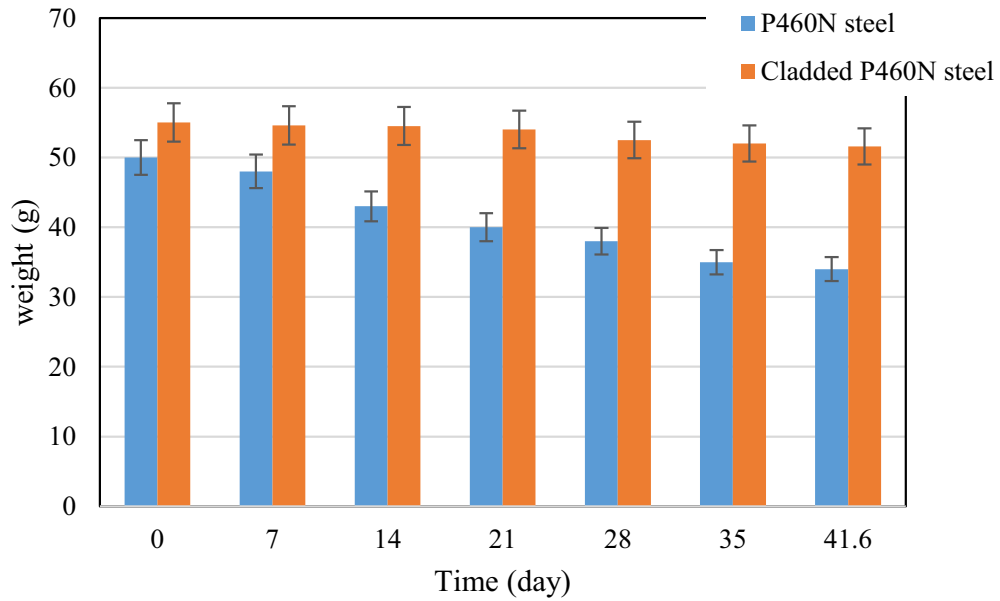
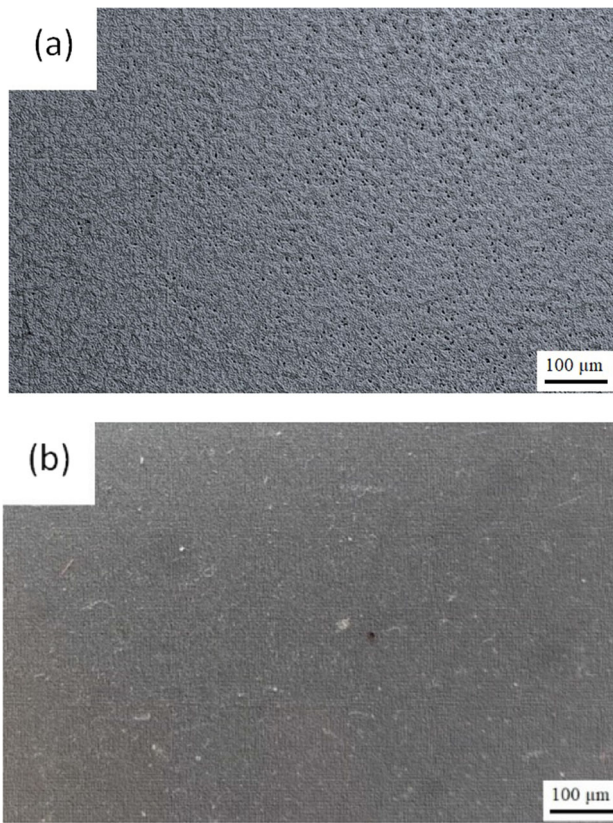Fig. 7—Weight changes of the immersed specimens in 1 M HCl solution.

Fig. 8—Microstructure of corroded specimens after the immersion test for 1000 h (*a*) base metal, (*b*) cladded specimen.
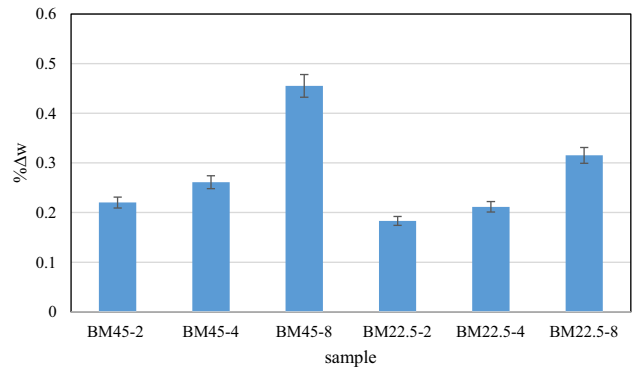

Fig. 9—Weight change percent for base metal samples after wear test.

D. *Wear Test*

1. *Effect of sliding and load value*

Figure 9 shows the effect of sliding and wear load value on the weight change percentage for P460N base metal. It can be seen that the weight change value has been enhanced significantly in high sliding values such as 800 m. Also, the amount of weight change decreased with the declining wear force as expected. However, the amount of weight change in BM45-8 is very significant compared to other samples. Examining the chart of friction coefficient *vs* sliding can greatly justify this phenomenon. The graphs of samples BM45-8 and BM45-4 are given in Figure 10. The friction coefficient
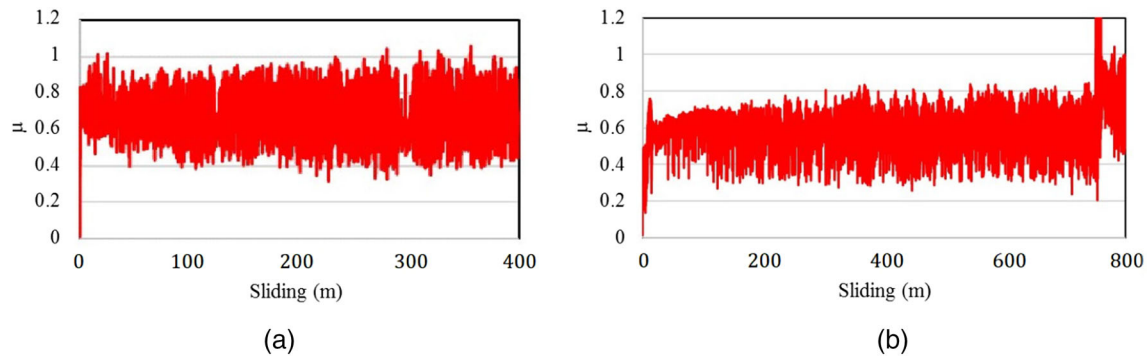
Fig. 10—Friction coefficient of (a) BM45-4 and (b) BM45-8.
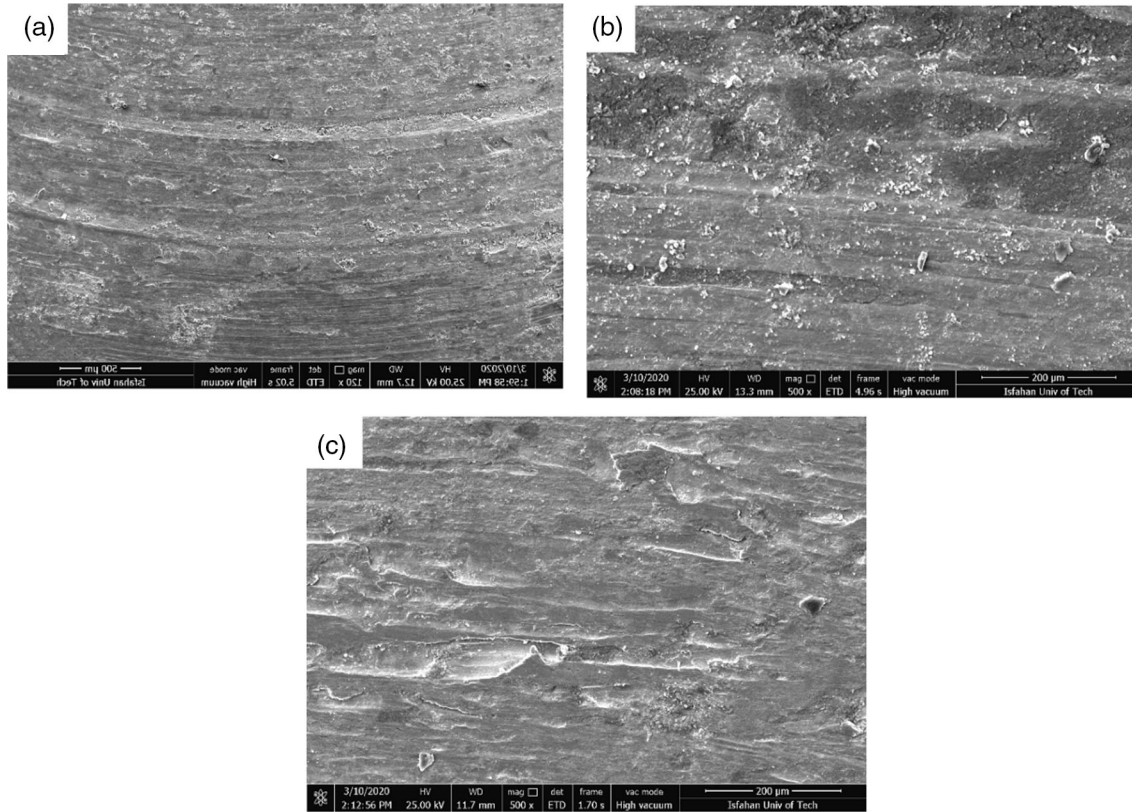

Fig. 11—The worn surface of (a) BM45-2, (b) BM45-4, and (c) BM45-8.

has suddenly increased, and the wear intensity has enhanced at about 750 m sliding. The formation of coarse abrasive particles has led to increased wear at this stage. Also, the placement of particles in the interface of the surfaces has intensified the friction coefficient. For further examination, SEM images of the worn surfaces of BM45-2, BM45-4, and BM45-8 are illustrated in Figure 11. In Figure 11(a), the presence of clear grooves indicates the formation of an abrasive wear mechanism in the BM45-2 specimen. In Figure 11(b), after 400 m of sliding, the intensity of abrasive wear has been reduced, and that of the adhesive wear has been added. The BM45-8 sample shows the severe wear caused by coarse abrasive particles. This phenomenon has exacerbated
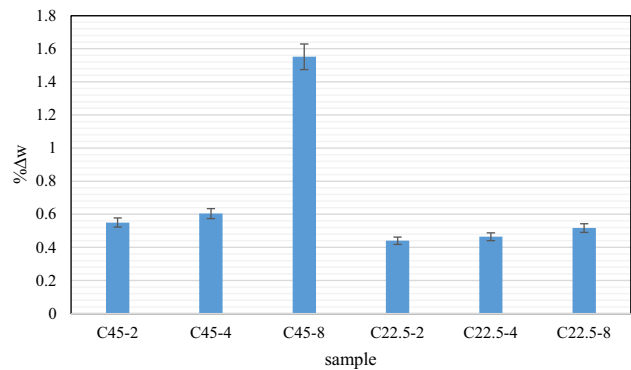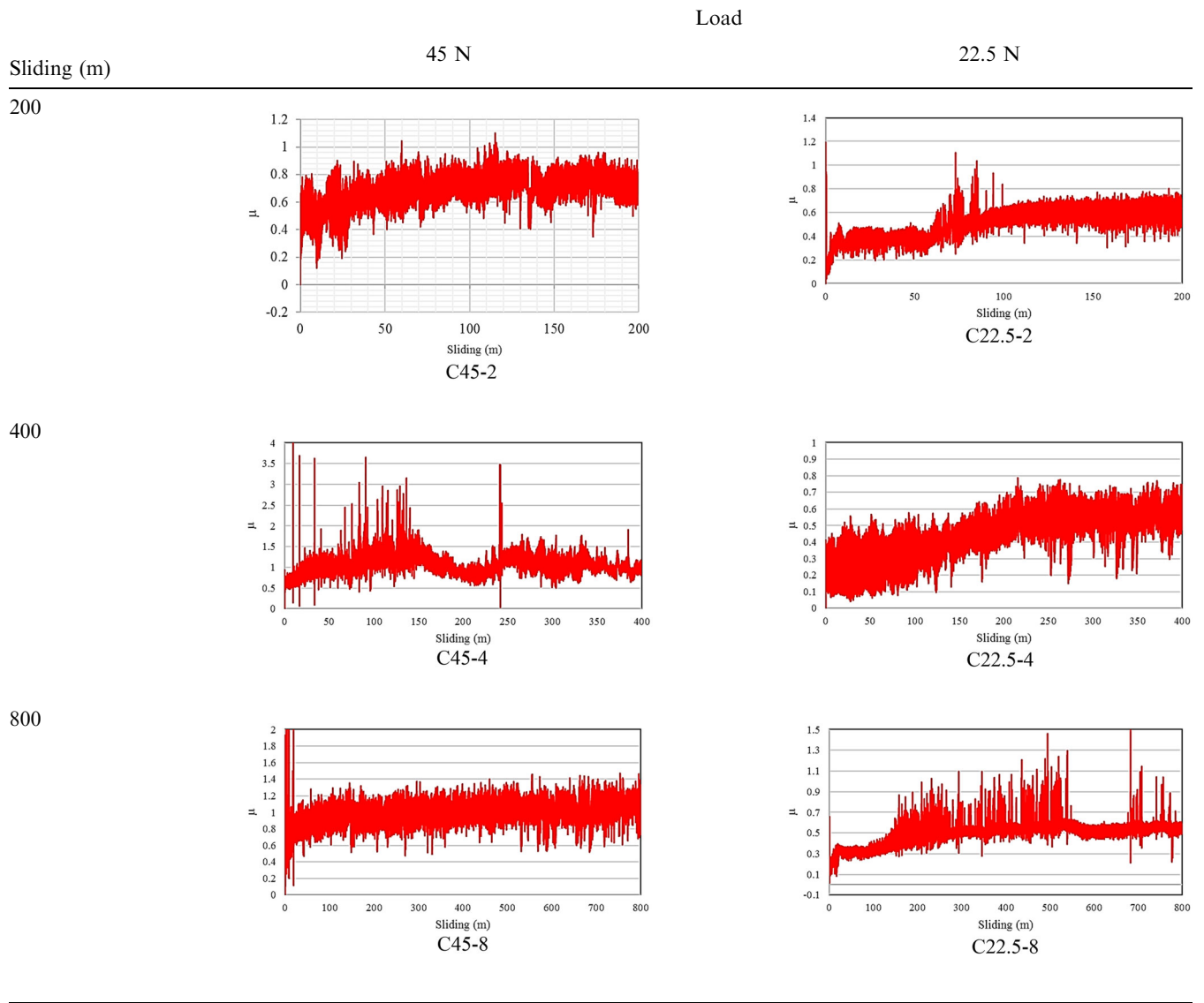

Fig. 12—Weight change percent for cladded samples after wear test.

Table VI. The Curve of Friction Coefficient of All Cladded Samples.

	Load	
Sliding (m)	45 N	22.5 N

C45-2

C22.5-2

C45-4

C22.5-4

C45-8

C22.5-8

high wear and severe weight loss in the BM45-8 sample. This result shows less intensity for those specimens with a lower load (BM22.5-2, BM22.5-4, and BM22.5-8).

The wear test results for cladded samples with Inconel 625 were different from the wear results for the base metal specimens. In Figure 12, the C45-8 specimen has shown the highest rate of weight change after the wear test. Under low loading conditions, the weight changes of the samples (C22.5-2, C22.5-4, and C22.5-8) were very low. For a better understanding, the friction coefficient curves of the cladded samples are shown in Table VI. The maximum and minimum friction coefficient values were for C45-8 and C22.5-8 specimens with about 0.89 and 0.39, respectively. It can be seen that the friction coefficient rises significantly once wear particles were formed at the wear surface, and particles presented in the interface affect the instantaneous friction coefficient and wear. These peaks are well illustrated in C45-4

and C22.5-8 specimens. However, the friction coefficient of the C22.5-8 sample is still low. The size of the separated particles was influenced by friction. In other word, the separated particle size of the C22.5-8 sample was smaller than that of the C45-4 sample. The fineness separated particles in C22.5-8 have led to the formation of lighter grooves and, in some cases, have led to polishing and lubricating effects, resulting in a reduction in the intensity of wear.

Figure 13 shows the worn surfaces of C22.5-2, C22.5-4, and C22.5-8 specimens. The worn surface of C22.5-2 has delamination wear with a deep scratch in some areas. In the C22.5-4 sample, the abrasive wear has replaced the delamination wear, and the cracks have been reduced. As the slip increases to 800 m (C22.5-8), wear particles become smaller, and as a result, wear rate decreases.
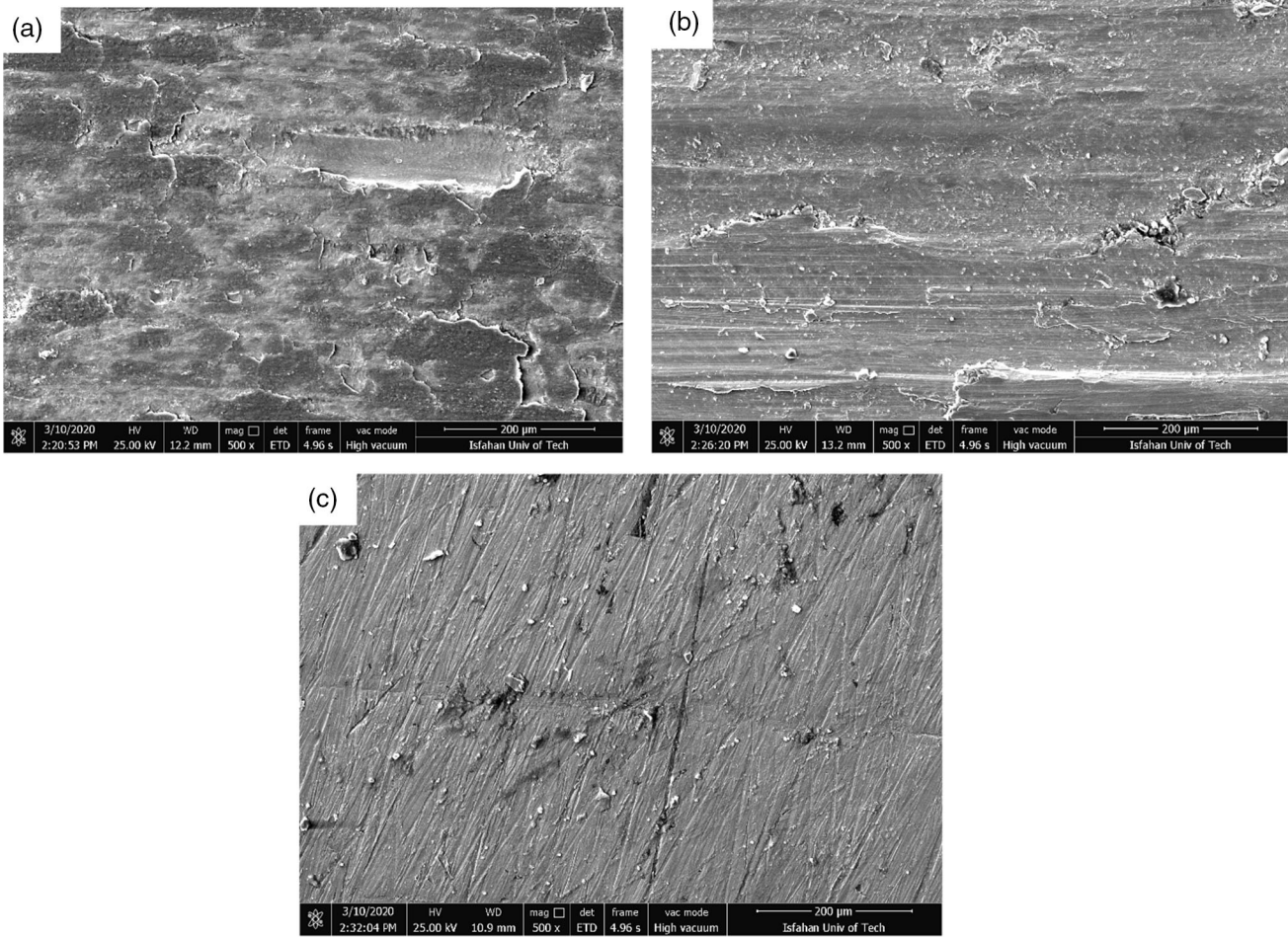
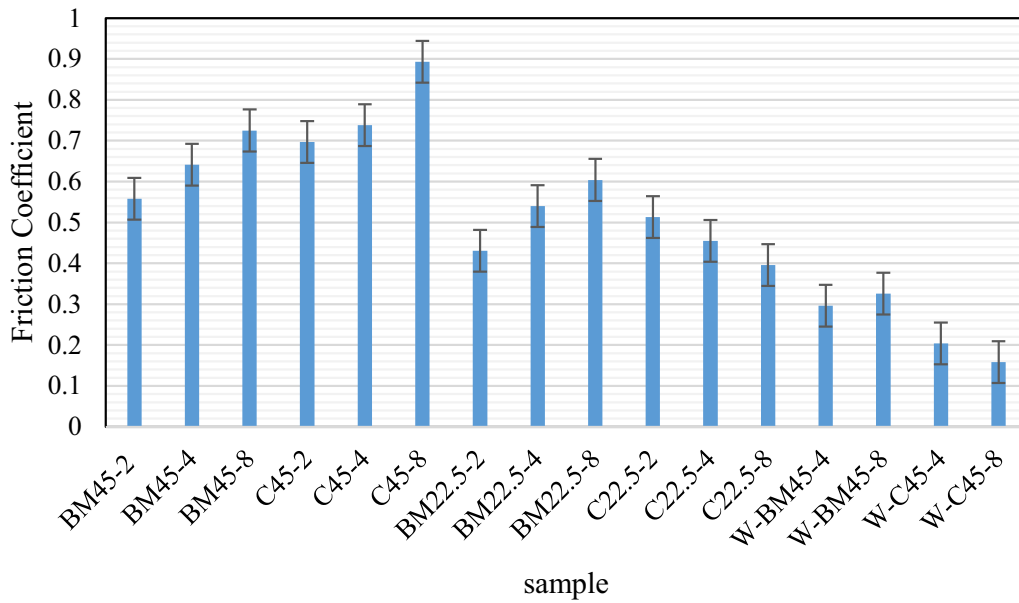Fig. 13—Worn surface of (*a*) C22.5-2, (*b*) C22.5-4, and (*c*) C22.5-8.

Fig. 14—Friction coefficient average of the same specimens in both environments, air and water.
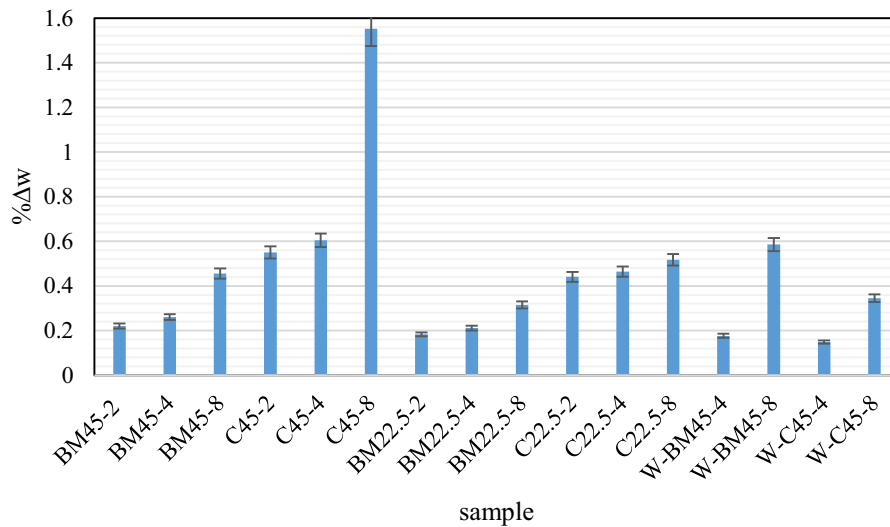
Fig. 15—Weight changing of the same specimens in both environments, air and water.
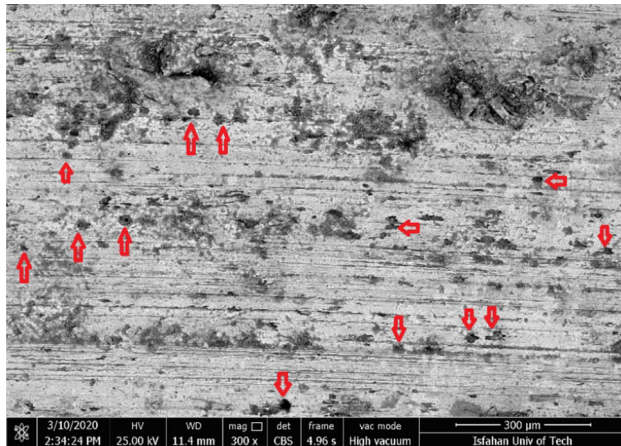

Fig. 16—The worn surface of W-BM45-8 sample..

A general comparison of the friction coefficients changes between base the metal and the cladded metal samples showed three-body abrasion in the cladded samples due to the separation of hard particles from the sliding surfaces. However, the cladded layer can be suitable for using at low wear forces (such as 22.5).

2. Effect of water environment

Such results strongly show that water could reduce the friction coefficient and wear volume; the wear loss is remarkably reduced in water. Figure 14 shows the average value of the friction coefficient of W-BM45-4 and BM45-2 under a 45 N load with and without a water environment. It can be seen that the existence of water has led to a reduction in the friction coefficient of the base metal. The amount of change in the friction coefficient has been more than 50 pct. Therefore, the effect of water in the abrasive environment for this alloy is negligible.

Besides, the comparison of wear test results between cladded samples and base metal was also interesting. The friction coefficient of the cladded samples has reached about 0.2 and has decreased to about 0.16, with the increasing distance in the aqueous environment.

The results of the weight changes in W-BM45-4 and BM45-2 are shown in Figure 15, which indicates a significant reduction in the weight loss of water-worn samples compared to air-worn samples. However, with the increase of sliding up to 800 m, the amount of weight loss has been increased to 0.34 pct. The latter result is slightly different for the base metal, with the weight change increasing by about 0.6 pct.

It can be concluded that the high hardness of the Inconel 625-cladded layer in the aqueous environment provides a better abrasion resistance. Furthermore, the study of the worn surfaces of different specimens illustrated that in the water environment, due to the increase in cavitation, the amount of destruction has been increased with the increase of sliding. According to Figure 16, the degradation due to cavitation is well observed in the W-BM45-8 sample.

A local increase in temperature and turbulence due to the sliding of the specimens during wear test has led to the formation and bursting of bubbles on the specimens' surface. The literature indicated that less attention has been paid to this phenomenon. Chen et al.[17] have also reported that the wear resistance in seawater environment has been decreased with increasing the normal load. One of the main reasons for this phenomenon could be the formation of bubbles in the interface of the wear surface, which has led to a decrease in friction and wear.

In summary, although the water environment leads to a decrease in the coefficient of friction, further destruction of the samples can happen due to cavitation. However, Inconel 625-cladded layer has been able to provide better wear resistance in water environment for its substrate, especially.

IV. CONCLUSION

This study was focused on the corrosion and wear behavior of cladded Inconel 625 on P460N steel fabricated by the GTAW process. The main conclusions were as follows:

1. The microstructure was composed of four different zones: the base metal and HAZ with proeutectoid ferrite and pearlite, the interface zone with Widmanstatten ferrites, the cladded layer with epitaxially grown dendrites with the average primary and secondary dendrite spacing of 17 and 9 μm. Some precipitations like Fe_xMo_y and $Cr_xFe_yNi_z$ were also detected in the weld zone.

2. The average hardness value of the cladded Inconel was about 2.5 times greater than that of the base metal. Also, the more uniform distribution of precipitate particles and elements at a depth of about 500 μm from the surface resulted in the maximum amount of hardness in the cladded layer.

3. The cladding of P460N steel enhanced its corrosion resistance in 3.5 wt pct NaCl water solution and the corrosion rate was reduced by about three times.

4. The wear resistance of the cladded Inconel 625 samples was enhanced in low loading forces compared to the base metal. However, increasing loading forces resulted in severe three-body abrasion. The cladding of P460N steel had provided more wear resistance in water environment by decreasing the friction coefficient, but cavitation destruction was observed in the surfaces of water-worn samples.

REFERENCES

1. K. Song, Z. Wang, S. Hu, S. Zhang, and E. Liang: *Mater. Manuf. Processes*, 2018, vol. 33, pp. 770–777.
2. M.N. Fesharaki, R. Shoja-Razavi, H.A. Mansouri, and H. Jamali: *Surf. Coat. Technol.*, 2018, vol. 353, pp. 25–31.
3. H.R.Z. Rajani and S.A.A.A. Mousavi: *Mater. Sci. Eng. A*, 2012, vol. 556, pp. 454–64.
4. O.P. Oladijo, V. Luzin, and T.P. Ntsoane: *Procedia Manuf.*, 2019, vol. 35, pp. 1234–39.
5. T.E. Abioye, J. Folkes, and A.T. Clare: *J. Mater. Process. Technol.*, 2013, vol. 213, pp. 2145–51.
6. B. Silwal, J. Walker, and D. West: *Int. J. Adv. Manuf. Technol.*, 2019, vol. 102, pp. 3839–48.
7. A. Evangeline and P. Sathiya: *Mater. Res. Express*, 2019, vol. 6, p. 106539.
8. G. Longlong, Z. Hualin, L. Shaohu, L. Yueqin, X. Xiaodong, and F. Chunyu: *Rare Met. Mater. Eng.*, 2016, vol. 45, pp. 2219–26.
9. M.N. Fesharaki, R. Shoja-Razavi, H.A. Mansouri, and H. Jamali: *Opt. Laser Technol.*, 2019, vol. 111, pp. 744–53.
10. J.F. Wang, Q.J. Sun, H. Wang, J.P. Liu, and J.C. Feng: *Mater. Sci. Eng. A*, 2016, vol. 676, pp. 395–405.
11. A. Iwabuchi: *Wear*, 1985, vol. 106, pp. 163–75.
12. H. Kashani, A. Amadeh, and H.M. Ghasemi: *Wear*, 2007, vol. 262, pp. 800–06.
13. G.R. Desale, C.P. Paul, B.K. Gandhi, and S.C. Jain: *Wear*, 2009, vol. 266, pp. 975–87.
14. G. Chakraborty, N. Kumar, C.R. Das, S.K. Albert, A.K. Bhaduri, S. Dash, and A.K. Tyagi: *Surf. Coat. Technol.*, 2014, vol. 244, pp. 180–88.
15. D. Verdi, M.A. Garrido, C.J. Munez, and P. Poza: *Mater. Des.*, 2015, vol. 67, pp. 20–27.
16. J. Wang, J. Chen, B. Chen, F. Yan, and Q. Xue: *Tribol. Int.*, 2012, vol. 56, pp. 38–46.
17. J. Chen, J. Wang, B. Chen, and F. Yan: *Tribol. Trans.*, 2011, vol. 54, pp. 514–22.
18. X. Xu, G. Mi, L. Chen, L. Xiong, P. Jiang, X. Shao, and C. Wang: *J. Alloys Compd.*, 2017, vol. 715, pp. 362–73.
19. K. Wang, B. Chang, J. Chen, H. Fu, Y. Lin, and Y. Lei: *Appl. Sci.*, 2017, vol. 7, p. 1065.
20. K.D. Ramkumar, A.J. Bhalodi, H.J. Ashokbhai, A. Balaji, S. Aravind, K.M. Aravind, and V. Varma: *J. Mater. Eng. Perform.*, 2016, vol. 26, pp. 5620–40.
21. J.S. Kim, Y.I.L. Park, and H.W. Lee: *Met. Mater. Int.*, 2015, vol. 21, pp. 350–55.
22. K.D. Ramkumar, W.S. Abraham, V. Viyash, N. Arivazhagan, and A.M. Rabel: *J. Manuf. Processes*, 2017, vol. 25, pp. 306–22.
23. L.Y. Xu, H.Y. Jing, and Y.D. Han: *Weld. World*, 2018, vol. 62, pp. 363–75.